crystals

MDPI

Article

Synthesis of MgFe Layered Double Hydroxide from Iron-Containing Acidic Residual Solution and Its Adsorption Performance

Alin Golban, Lavinia Lupa *, Laura Cocheci * and Rodica Pode

Politehnica University of Timisoara, Faculty of Industrial Chemistry and Environmental Engineering, 6 Vasile Parvan Blvd., Timisoara 300223, Romania; rodica.pode@upt.ro

* Correspondence: lavinia.lupa@upt.ro; laura.cocheci@upt.ro; Tel.: +402-5640-4159

Received: 19 August 2019; Accepted: 1 October 2019; Published: 3 October 2019

Abstract: The paper presents a new method of layered double hydroxide (LDH) synthesis starting from secondary sources, namely acidic residual solutions. The iron content of the acidic solution resulting from the pickling step of the hot-dip galvanizing process make it suitable to be used as an iron precursor in LDH synthesis. Here, Mg_4Fe–LDH synthesized through the newly proposed method presented structural and morphological characteristics similar to the properties of layered double hydroxides synthesized from analytical-grade reagents. Moreover, the as-synthesized LDH and its calcined product presented efficient adsorption properties in the removal process of Mo(VI) from aqueous solutions. The adsorption studies are discussed from the equilibrium, kinetic, and thermodynamic points of view. The proposed novel technologies present both economic and environmental protection benefits.

Keywords: iron precursor; acidic residual solution; LDH synthesis; Mo(VI) adsorption

1. Introduction

Concerns over water resource pollution are continuously increasing, which has intensified research efforts regarding water decontamination. Because issues arise when the contaminants are in trace amounts but still at a concentration which exceeds the maximum admitted values, one of the most studied water treatment methods is adsorption. The adsorption process has gained researchers' interest due to its simple operating conditions and the versatile types of adsorbent materials which exist on the market [1–3]. Among the multitude of adsorbent materials, a considerable amount of attention has been paid to layered double hydroxide (LDH) compounds. The general formula of an LDH is $[M^{II}_{1-x}M^{III}_{x}(OH)_2]^{x+}$. $[A^{n-}_{x/n} \cdot mH_2O]^{x-}$, where M^{II} is a divalent cation, M^{III} is a trivalent cation, and A^{n-} is an anion. Their lamellar structure is based on brucite-like sheets, where some divalent cations are replaced with trivalent cations, resulting in some positively charged layers that contain between them various anions such as CO_3^{2-}, Cl^-, NO_3^-, or even organic anions [4,5]. This structure increases their adsorptive properties, especially if the contaminant is in the form of oxyanions [6–8]. Due to the positive charge of the brucite-like lamellar layers, one of the main properties of synthetized LDHs is anionic exchange. If the LDH is thermal treated at temperatures up to 600 °C, when the obtained mixed metal oxides are immersed in aqueous solution, they are able to rehydrate and restore the lamellar structure of the LDH while retaining the anions present in solution in order to provide a neutral LDH molecule. This property is referred to as the "memory effect" and it is most often utilized to treat water containing undesirable anions or to introduce various anions into the LDH structure. From the multitude of Me^{2+}/Me^{3+} LDH types, much focus has been directed toward the Mg^{2+}/Fe^{3+} pair. A literature search revealed that Mg/Fe–LDH has been used for phosphate removal from aqueous

solutions [9–11]; as adsorbent materials of various heavy metals, such as Cr, As, Pb, Zn, Cu, Se, Sb, and so forth [12–16]; for treatment of aqueous solutions contaminated with different reactive dyes [17–19]; or as a catalyst [20–22].

Presently, there is a focus on obtaining cheaper adsorbent materials that still retain properties similar to those obtained from pure chemicals. Therefore, the tendency is to replace some raw materials with secondary sources of various metals. This helps reduce production costs as well as protect the environment by recycling and recovering various waste products. To this end, some researchers have studied the possibility of obtaining LDHs by using, as a precursor of various metal ions, different industrial wastes, such as fly ash, zinc ash, furnace slag, aluminum slag, and so forth. [23–27]. In most cases, the wastes were used as precursors for magnesium, zinc, or aluminum ions. However, even though the obtained LDHs presented very good properties similar to LDHs obtained from reagents and the process helped the environment by recycling wastes, there were no significant reductions in the production cost. In all of these cases, the precursor was a solid waste, which first needed to be brought into solution. This required the use of some acid solutions and added an extra step in the LDH production process.

Therefore, in the present study, we present a new Mg/Fe–LDH obtained from secondary sources using, for the first time, an acidic residual solution resulting from the pickling step in the hot-dip galvanizing process as an iron precursor. In a previous study, we demonstrated that an Mg/Fe–LDH obtained using a secondary source as an iron precursor (iron sludge resulting from the hot-dip galvanizing process) presented properties similar to those obtained from reagents [28]. The novelty of this method is that, by directly using an acidic waste solution as an iron precursor, two steps are avoided in the process of obtaining LDHs. First, the acidic solution from the hot-dip galvanizing process is not neutralized in order to obtain the sludge, and second, the hydrometallurgical leaching of sludge is avoided when obtaining the iron precursor. In order to determine the efficiency of using the acidic residual solution as an iron precursor in the process of obtaining Mg/Fe–LDH, the LDH was analyzed and used as an adsorbent material in the removal process of Mo(VI) as molybdate (MO_4^{2-}) from aqueous solutions.

Due to the extensive use of Mo(VI) in many practices, molybdate anions (MO_4^{2-}), the most common oxyanions of Mo(VI), can be found in various waste waters, such as mining waters, scrubber effluent of municipal solid waste incinerators, waste waters from the production of stainless-steel or cast iron alloys, and waste water from the production of various pigments and catalysts for high-temperature chemical processes [29–31]. If molybdenum is present in drinking water at a level higher than 0.07 mg/L, which is the maximum value admitted by the World Health Organization (WHO) [32], it could be toxic to animals and humans [33]. Therefore, finding an efficient method to remove oxyanions from aqueous solutions is still a challenge, taking into account the fact that the traditional method of waste water treatment, precipitation, can remove only cations and not oxyanions [30]. There are few papers which report the removal of Mo(VI) from aqueous solutions involving an ionic exchange mechanism using various LDHs synthesized from pure reagents [7,8,34]. The purpose of this study was to compare the adsorption performance of the new, synthesized LDH from a secondary iron source with those reported in the literature.

2. Experimental

2.1. Mg/Fe–LDH Synthesis and Characterization

The acidic residual solution was received from a local hot-dip galvanizing plant and was subjected to chemical analysis in order to determine the metal ion concentrations. The concentration of Fe^{2+} was determined through titration with $KMnO_4$. The concentrations of total iron and other ions present in solution were determined by atomic absorption spectrometry using a Varian SpectrAA 280 FS spectrophotometer (Agilent, Santa Clara, CA, USA).

Mg/Fe–LDH was synthesized using the coprecipitation method at low oversaturation [4]: 200 mL of 1 M solution containing iron residual solution and magnesium nitrate, at a Mg:Fe molar ratio of 4:1, was added dropwise under continuous stirring to 100 mL of 1 M Na_2CO_3 solution. The pH of the suspension was maintained in the range of 10–11 using a 2 M NaOH solution. The suspension was aged at 70 °C for 20 h, then filtered and washed with distilled water several times until reaching a pH of 7. The obtained slurry was dried overnight, then milled and sieved in order to obtain particles with dimensions less than 90 μm, which were used in this study. A portion of the obtained Mg_4Fe–LDH was calcined at 450 °C at a heating rate of 10 °C/min. It was maintained at this temperature for 3 h using a Nabertherm oven. The obtained material was named Mg_4Fe-450.

The as-synthesized sample and the calcined one were characterized by powder X-ray diffraction (XRD), scanning electron microscopy (SEM), X-ray dispersion analysis (EDX), and specific surface area and pore volume. The RX diffractograms were recorded using a Rigaku Ultima IV X-ray diffractometer (Rigaku Analytical Devices Inc., Wilmington, MA, USA). SEM images were recorded using a Quanta FEG 250 microscope (FEI Company, Hillsboro, OR, USA) equipped with a ZAF-type EDX quantifier (FEI Company). A Micromeritics ASAP 2020 instrument (Micromeritics, Norcross, GA, USA) was used to determine the specific surface area and pore volume of the studied samples.

In order to determine the adsorption performance of the obtained materials, both samples—the as-synthesized LDH (Mg_4Fe) and the calcined one (Mg_4Fe-450)—were used in experiments to remove Mo(VI) from aqueous solutions.

The resulting adsorbent after Mo(VI) adsorption was analyzed using an FEI Tecnai F20 G2 TWIN TEM (FEI Company) at an accelerating voltage of 200 kV in bright field mode in order to determine the morphology.

2.2. Adsorption Studies

Both materials, the as-synthesized and the calcined samples, were used in the removal process of Mo(VI) anions from aqueous solutions. The adsorption process was conducted in batch mode using a Julabo SW23 shaker for sample shaking at a constant rotation speed (200 rpm). The adsorption performance of the obtained materials developed in the removal process of Mo(VI) anions from aqueous solutions was studied taking into account the influence of the Mo(VI) initial concentrations (15–200 mg/L), stirring time (5–240 min), and temperature (20, 35, and 50 °C). For all the adsorption studies, the solid:liquid ratio between the adsorbent and Mo(VI)-containing aqueous solutions was 0.025 g in 25 mL (i.e., solid:liquid ratio (S:L) = 1 g/L). The initial pH of the solution was adjusted to pH = 6.0 ± 0.5. According to the literature review and our previous studies [2,35], Mo(VI) adsorption onto LDHs is maximal at this pH due to the fact that, at this value, Mo(VI) is found in the solution under MoO_4^{2-}.

After each adsorption experiment, the samples were filtered in order to separate the phases and to analyze the residual concentration of Mo(VI). The Mo(VI) concentration before and after adsorption was determined through atomic absorption spectrometry using a Varian SpectrAA 280 FS spectrometer.

The mass balance presented in Equation (1) was used for the calculation of Mo(VI) uptake on 1 g of adsorbent:

$$q_e = \frac{(C_0 - C_e) \cdot V}{m} \quad (1)$$

where q_e is the adsorbed quantity of Mo(VI), expressed in milligrams per 1 g of studied adsorbent; C_o and C_e represent the Mo(VI) concentration of the aqueous solutions before adsorption and after the established equilibrium (mg/L); V is the volume of the Mo(VI)-containing aqueous solution (L); and m is the mass of the Mg_4Fe–LDH (g) used in the experiments.

3. Results and Discussions

3.1. Material Characterizations

It is estimated that, in the European Union, almost 300,000 m^3 of acidic residual solution is produced annually in the hot-dip galvanizing industry. [36] Due to its corrosive nature and high concentration of metal ions, this solution is considered a toxic waste and requires treatment before dumping. The treatment processes for spent pickling solutions can be classified as neutralization treatments, treatments for acid recovery, and treatments for metal recovery. Neutralization treatments consist of adding NaOH or $Ca(OH)_2$ when the metal ions are precipitated, and the resulting sludge is dried and considered a solid waste. Treatment processes for acid recovery include evaporation, membrane processes (membrane dialysis, membrane electrolysis, and membrane distillation), and processes with fluidized beds (Ruthner or spray-roasting processes). Metal ion recovery can employ ion exchange, crystallization, or solvent extraction. The physicochemical characterization of the acidic residual solution resulting from the pickling step of the hot-dip galvanizing process is presented in Table 1. It can be observed that the residual solution contains a high concentration of iron (65 g/L), which makes it suitable to be used as an iron precursor in LDH synthesis. The concentration of iron ions in the residual solutions can be considered constant because these acidic solutions resulting from the pickling step in the hot-dip galvanizing industry are continuously analyzed, and when they achieve the maximum value of iron ions and the minimum value of acidity, they are removed from the process and can be used as a secondary source of iron ions for LDH manufacturing applications. Besides iron ions, the residual solution also contains other metal ions, but in a smaller concentration; their presence does not inhibit the synthesis of LDHs.

Table 1. Physicochemical characterization of the acidic residual solution.

No.	Parameter	Value
1.	pH	2.15
2.	Fe	65.0 g/L
3.	Cu	57.4 mg/L
4.	Cd	0.453 mg/L
5.	Pb	15.2 mg/L
6.	Zn	565 mg/L
7.	Cl^-	81.7 g/L
8.	TOC	68 mg/L

The XRD patterns of the obtained adsorbent are presented in Figure 1. It can be observed that the Mg_4Fe obtained from a secondary source of iron showed a unique main phase which corresponded to pyroaurite. The cell parameters a and c were calculated using Bragg's law, assuming a rhombohedral symmetry of crystallization. The cell parameter a represents the cation–cation distance within the brucite-like layer ($a = 2 \cdot d_{(110)} = 3.11$ Å) and c represents the adjacent distance of the hydroxide layer ($c = 3 \cdot d_{(003)} = 23.9$ Å), where $d = \lambda/2 \sin \theta$ and $\lambda = 1.54056$ Å. The obtained results are in good agreement with other results reported by several authors [19,28,37]. The impurities present in the acidic residual solution were under 5% and they did not lead to the formation of secondary phases in the Mg_4Fe–LDH structure. In the case of the sample calcined at 450 °C, the LDH structure was modified, and the RX diffractogram was specific to a poor crystalline phase corresponding to MgO (periclase), with Fe^{3+} probably dispersed in the structure. Due to smaller Fe^{3+} than Mg^{2+} concentration utilized in the starting solution and the low temperature of the thermal treatment (450 °C) of Mg_4Fe, it was difficult to achieve the formation of iron oxide species such as magnesioferrite ($MgFe_2O_4$) or maghemite (Fe_2O_3). At this calcination temperature, the iron oxides were amorphous and the crystals

were in the course of forming; therefore, they could not be identified by the RX analysis. These findings are also in agreement with other results reported in the literature [37,38]. For this reason, it is expected that this sample has the highest adsorption capacity in the removal process of Mo(VI) anions from aqueous solutions [19,28].

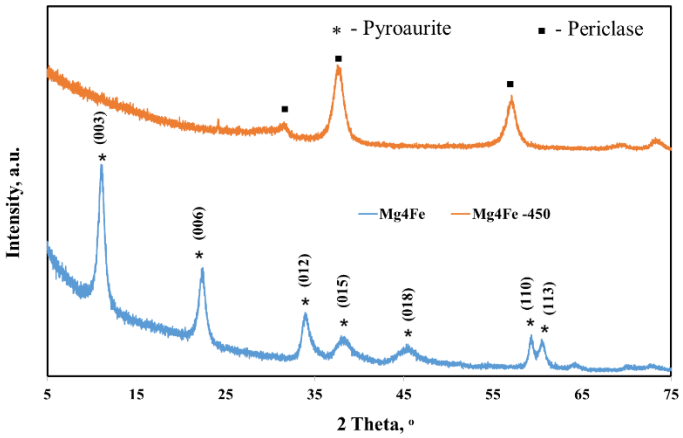

Figure 1. XRD pattern of the synthesized materials.

The morphology of the synthesized samples can be observed from the SEM images presented in Figure 2. The Mg_4Fe–LDH presented an aerated structure of fluffy particles. Through calcination, the sample became more amorphous, and the surface had aspects of cotton flowers.

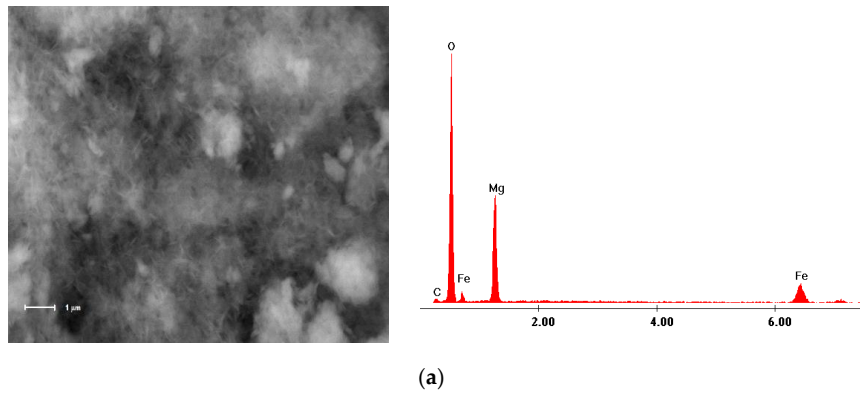

(**a**)

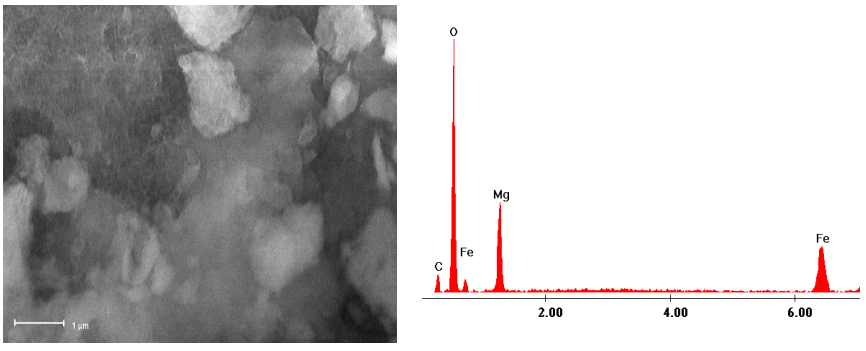

(**b**)

Figure 2. SEM images and X-ray dispersion analysis (EDX) spectra of the synthesized samples: (**a**) Mg_4Fe and (**b**) Mg_4Fe–450.

The EDX spectra presented in Figure 2 show the peaks of the characteristic elements of the studied materials. No characteristic peaks appeared for the impurities present in the precursor solution. This indicates that there was a negligible quantity of impurities.

The molar ratio between Mg and Fe ions from the studied samples together with their BET specific surface area and pore volume are presented in Table 2.

Table 2. Physical and chemical properties of the studied samples.

Parameters		Mg_4Fe	Mg_4Fe–450
Molar ratio	Theoretical	4	4
	Experimental	3.98	4.08
S_{BET} (m^2/g)		101	0.536
V_p (cm^3/g)		192	0.802
Cd, %		0.16	0.08
Pb, %		0.12	0.22
Zn, %		1.19	1.59

The impurities present in the spent pickling solution were analyzed in the washing solutions of the LDH in the as-synthesized solid samples and the calcined one and in the solutions after Mo(VI) adsorptions. It can be observed from the chemical analysis that impurities could be found in the solid synthesized samples but in a concentration under 2%, this being the reason why these do not appear in the EDX and RX analyses, as they are under the detection limit of 5%. Impurities could not be detected in the washing waters of the synthesized Mg_4Fe–LDH and in the residual solutions after Mo(VI) adsorption. This demonstrates that the impurities were not released during the adsorption process from the solid support.

3.2. Equilibrium Studies

The equilibrium isotherms representing the dependence of the adsorption capacities developed by the Mg_4Fe and Mg_4Fe-450 as a function of the Mo(VI) concentrations at equilibrium are presented in Figure 3. Increasing the initial concentration of Mo(VI) increased the active sites available for adsorption and, therefore, increased the adsorption capacities of both the studied materials. Mg_4Fe developed an experimental maximum adsorption capacity in the removal process of Mo(VI) from aqueous solutions of 39.9 mg/g. Further, due to the memory effect, the calcined samples exhibited a higher experimental maximum adsorption capacity of almost 50% (q_e = 52.8 mg/g). For aqueous solutions with Mo(VI) initial concentrations of ≤30 mg/L, the removal degree of Mo using a S:L ratio of 1 g/L was higher than 90%. For aqueous solutions with higher Mo(VI) initial concentrations, in order to obtain higher removal degrees, it was necessary to increase the S:L ratio. Other studies reported in the literature also present higher adsorption capacities for calcined samples compared with synthesized samples [18,28].

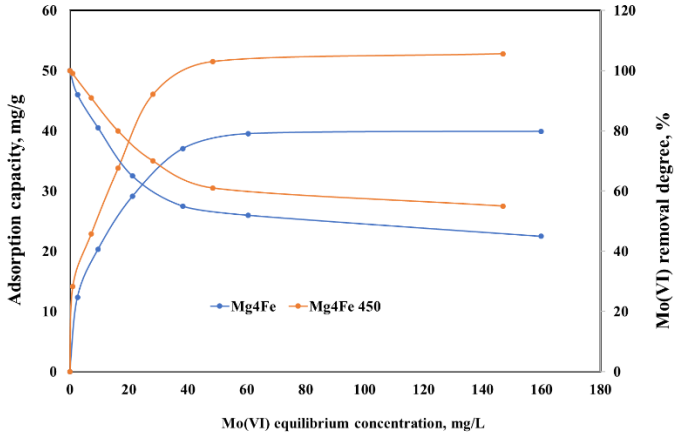

Figure 3. Equilibrium isotherms of Mo(VI) adsorption onto Mg_4Fe and Mg_4Fe-450. S:L = 1 g/L, t = 60 min, pH = 6, T = 20 °C.

Every adsorption study aims to determine the maximum adsorption capacity of the studied adsorbents and the equilibrium coefficient in order to achieve the design. Therefore, several isotherms, such as Langmuir, Freundlich, Temkin, and Dubinin–Radushkevich (DR) isotherms in their linear form, have been employed for this purpose [2,18,39]. The Langmuir isotherm supposes that the adsorption process takes place in a single layer on a uniform surface containing equivalent sites of the studied adsorbents. The Freundlich isotherm is used to express the affinity of the studied adsorbent to the retained pollutant. If the adsorption data fit the Temkin isotherm well, this means that the adsorbent surface is heterogeneous. In order to design the equilibrium adsorption regarding Mo(VI) removal using Mg_4Fe and Mg_4Fe-450, the linear graphs of the mentioned isotherms were plotted (Figure 4) and the obtained equilibrium isotherm parameters together with the regression coefficients are presented in Table 3.

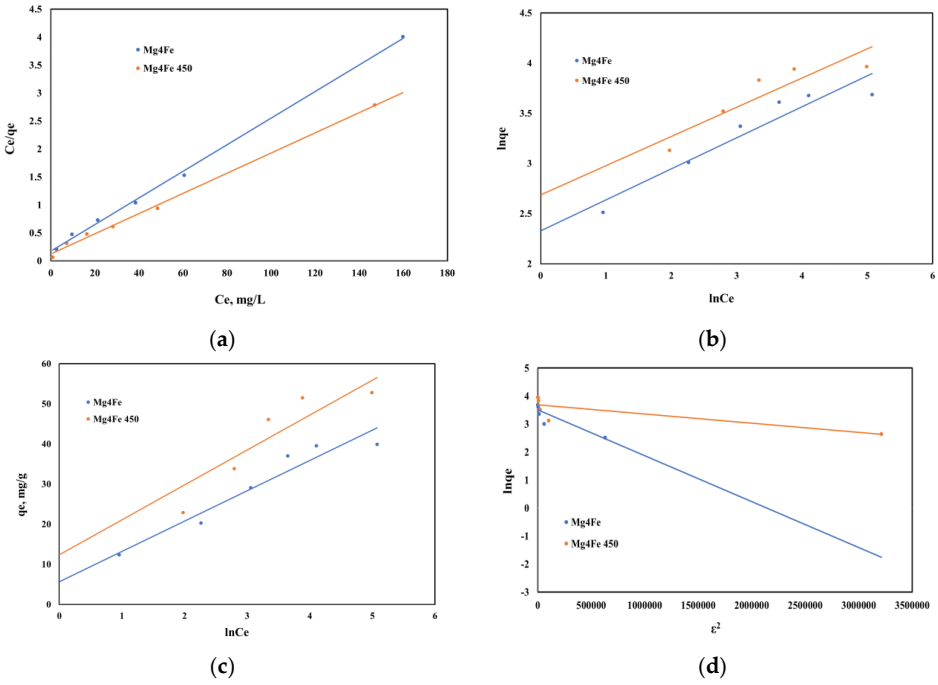

Figure 4. Equilibrium isotherms of Mo(VI) adsorption onto the studied adsorbent: (**a**) Langmuir, (**b**) Freundlich, (**c**) Temkin, and (**d**) Dubinin–Radushkevich.

Table 3. Equilibrium sorption isotherm parameters for Mo(VI) adsorption onto Mg_4Fe and Mg_4Fe-450.

Type of Isotherm	Parameter	Adsorbent	
		Mg_4Fe	**Mg_4Fe-450**
Langmuir	K_L, L/mg	0.137	0.151
	q_m calc, mg/g	42.1	55.2
	R^2	0.9981	0.9964
Freundlich	K_F, mg/g	9.33	14.7
	1/n	0.3086	0.2908
	R^2	0.9112	0.9330
Temkin	K_T, L/g	1.006	1.016
	b_T, J/mol	875	758
	R^2	0.9286	0.9074
Dubinin–Radushkevich	K_{ad}, mol^2/kJ^2	2×10^{-6}	3×10^{-7}
	q_s, mg/g	33.2	40.04
	R^2	0.7725	0.6644

Both studied materials presented affinity for Mo(VI) ion removal (1/n parameters were below unity).

By comparing the equilibrium isotherm parameters presented in Table 3, it can be concluded that Mo(VI) removal from the aqueous solutions occurred as a monolayer at the uniform surfaces of the Mg_4Fe and Mg_4Fe-450 materials because the Langmuir isotherm obtained the highest regression coefficients (closed to unity). Further, there was no significant difference between the maximum adsorption capacity calculated from its plot and those determined experimentally.

The lowest regression coefficients were obtained for the DR plots. At the same time, different values were obtained for the monomolecular adsorption capacities q_s for the studied materials and the values experimentally obtained in the adsorption process of Mo(VI) removal from aqueous solutions. The results suggest that the DR plot cannot be used to model the adsorption data of MoO_4^{2-} onto Mg_4Fe and Mg_4Fe-450 [18,39].

3.3. Kinetic Studies

Kinetic studies were used to determine the optimum time necessary to establish the equilibrium between the Mg_4Fe–LDH and the Mo(VI) anions. The experiments regarding the various stirring times were conducted at three different temperatures (Figure 5). Mo(VI) removal occurred quite quickly in the first minutes of contact between the adsorbent and adsorbate, especially when the calcined sample was used. After 60 min of stirring, the adsorption capacity increased slowly, so it can be considered that equilibrium was achieved in 60 min at all the studied temperatures for both adsorbent materials. The temperature increase led to a slight increase of the adsorption capacity of Mg_4Fe and Mg_4Fe-450 in the removal process of Mo(VI).

The well-known models of pseudo-first-order, pseudo-second-order, and intraparticle diffusion were used to simulate the kinetics of Mo(VI) adsorption onto the studied materials [18,19,40]. The representations of their linear plots are presented in Figures 6–8, and the kinetic parameters together with the obtained correlation coefficients are summarized in Table 4. From the linear representation of the experimental data according to the pseudo-first-order and pseudo-second-order kinetic models (Figures 6 and 7) and the interpretation of their parameters (Table 4), it can be concluded that Mo(VI) adsorption onto Mg_4Fe and Mg_4Fe-450, separately, is best described by the pseudo-second-order kinetic model. In this case, for all three temperatures, correlation coefficients were obtained that were close to 1, and the calculated adsorption capacities were similar to those determined experimentally.

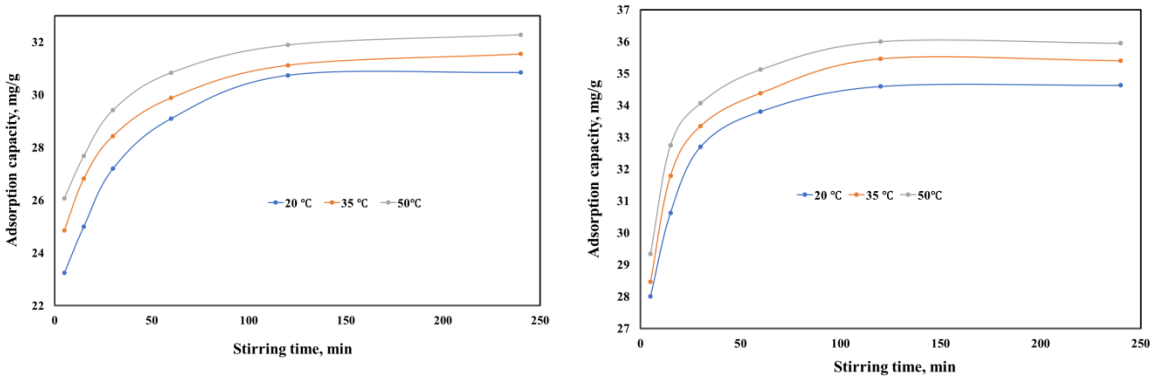

Figure 5. Effect of contact time on the adsorption capacity of (**a**) Mg_4Fe and (**b**) Mg_4Fe-450 at three different temperatures in the removal process of MoO_4^{2-} from aqueous solutions. S:L = 1 g/L, C_0 = 50 mg/L Mo(VI), pH = 6.

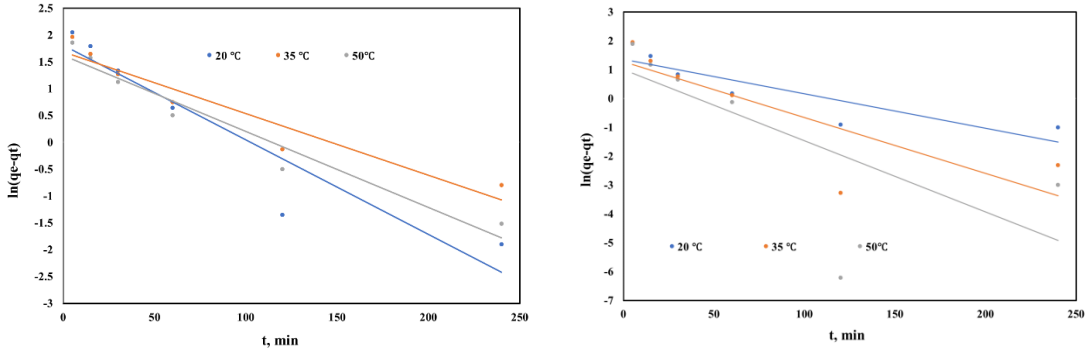

Figure 6. Pseudo-first-order kinetic model of MoO_4^{2-} adsorption onto (**a**) Mg_4Fe and (**b**) Mg_4Fe-450.

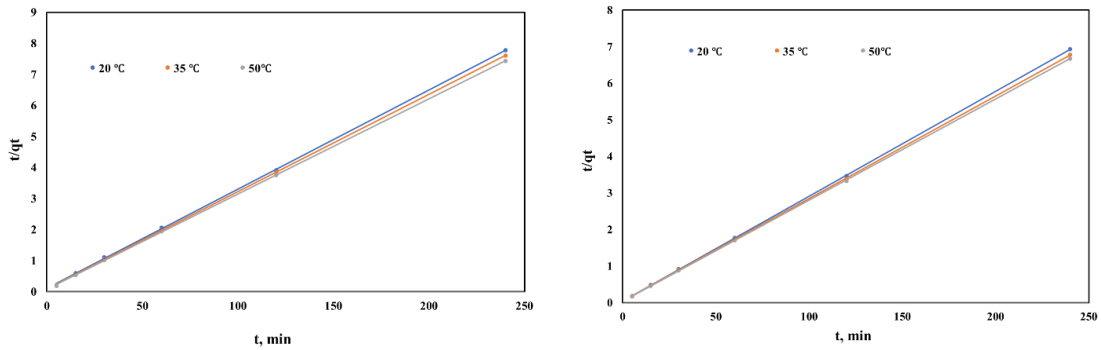

Figure 7. Pseudo-second-order kinetic model of MoO_4^{2-} adsorption onto (**a**) Mg_4Fe and (**b**) Mg_4Fe-450.

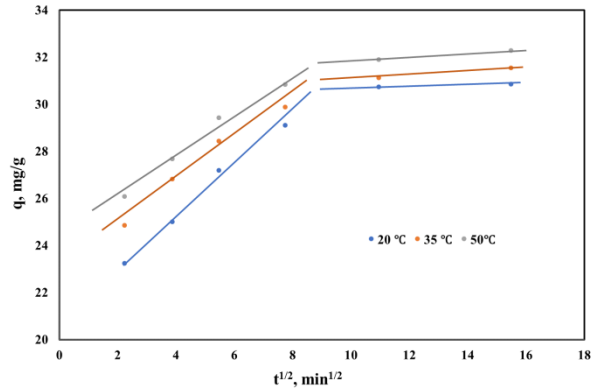

(**a**)

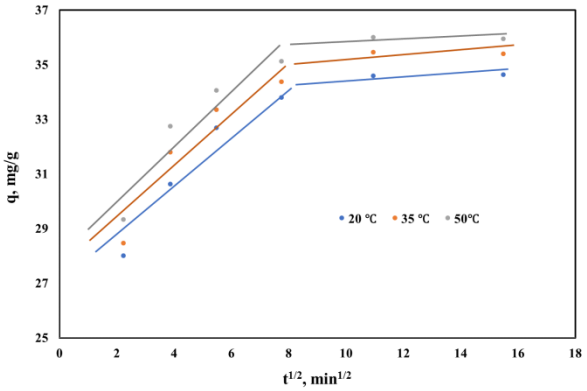

(**b**)

Figure 8. Intraparticle diffusion model of MoO_4^{2-} adsorption onto (**a**) Mg_4Fe and (**b**) Mg_4Fe-450.

Table 4. Kinetic model parameters for Mo(VI) adsorption onto Mg_4Fe and Mg_4Fe-450.

Model	Parameter	Adsorbent					
		Mg_4Fe			Mg_4Fe-450		
		Temperature			Temperature		
		20 °C	35 °C	50 °C	20 °C	35 °C	50 °C
	$q_{e\ exp}$, mg/g	31	32	32.5	35	35.5	36
Pseudo-first-order	K_1, min^{-1}	0.0176	0.0115	0.0142	0.0120	0.0194	0.0247
	q_e calc, mg/g	6.095	5.37	5.04	3.91	3.59	2.72
	R^2	0.8887	0.9189	0.9478	0.7772	0.6894	0.5104
Pseudo-second-order	K_2, min/(mg/g)	0.00934	0.0109	0.0119	0.0137	0.0163	0.0185
	q_e calc, mg/g	31.4	31.8	32.6	35	35.7	36.2
	R^2	0.9998	0.9999	0.9999	0.9999	0.9999	0.9999
Intraparticle diffusion	K_{int}	1.082	0.909	0.874	1.051	1.038	1.004
	R^2	0.9905	0.9777	0.9850	0.9356	0.8901	0.8780

The pseudo-second-order kinetic model can be used to simulate the experimental data regarding MoO_4^{2-} adsorption onto the studied materials; this means that the process is controlled by a chemical sorption [19,40,41].

Through the simulation of the experimental data according to the intraparticle diffusion model (Figure 8), it can be observed that the straight line does not pass through origin, indicating that the rate-limiting step for Mo(VI) adsorption is not the intraparticle diffusion. Also, the straight line presents a fragmentation after a while, suggesting that the adsorption process is more complex. The fast removal

of Mo(VI) in the first minutes of contact between the adsorbent and adsorbate was controlled by the film diffusion when the studied adsorbent surfaces were covered with MoO_4^{2-} anions. After the surface coverage, the transportation of Mo(VI) inside the adsorbent particles occurred, as suggested by the second straight line obtained through the representation of q versus $t^{1/2}$ (Figure 8) [19].

3.4. Thermodynamic Studies

From the linear plot representation of the Arrhenius equation ($\ln(K_2)$ versus 1/T, Figure 9), the activation energy of Mo(VI) adsorption onto the studied materials was determined. The activation energy value confers information regarding the type of adsorption process (physical, when E < 4.2 kJ/mol, or chemical, when E > 4.2 kJ/mol) [33]. The activation energy determined for MoO_4^{2-} sorption onto Mg_4Fe and M_4Fe-450 was determined to be 6.37 and 7.89 kJ/mol, respectively, indicating chemisorption (Table 5).

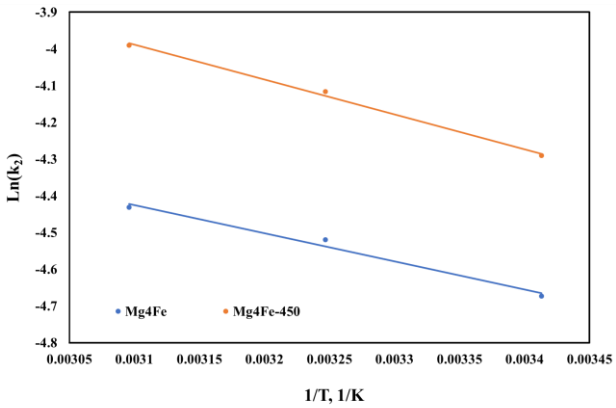

Figure 9. Arrhenius plot of MoO_4^{2-} adsorption onto the studied materials.

Table 5. Thermodynamic parameters for Mo(VI) adsorption onto Mg_4Fe and Mg_4Fe-450.

Parameter		Adsorbent	
		Mg_4Fe	**Mg_4Fe-450**
E, kJ/mol		6.37	7.89
ΔH^o, kJ/mol^{-1}		3.35	2.14
ΔS^o, J/(mol · K)		15.3	14.4
R^2		0.9869	0.9997
ΔG^o, kJ/mol	293 K	−1.13	−2.15
	308 K	−1.36	−2.30
	323 K	−1.59	−2.51

The thermodynamic equilibrium constant K_d, defined as the ratio between the Mo(VI) concentration in the solid phase and the solution at equilibrium, was used to calculate the Gibbs free energy (ΔG^o) at the studied temperatures and for the van 't Hoff representation in order to determine the thermodynamic parameters enthalpy (ΔH^o) and entropy (ΔS^o) for MoO_4^{2-} adsorption onto the studied materials [19,40,41]. The plot of the van 't Hoff representation is shown in Figure 10 and the thermodynamic parameters are listed in Table 5.

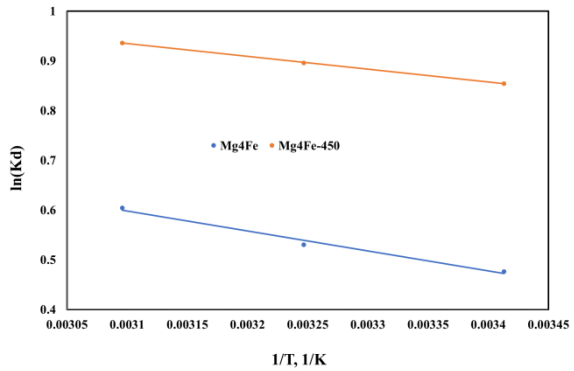

Figure 10. Van 't Hoff plot of MoO_4^{2-} adsorption onto the studied materials.

The MoO_4^{2-} adsorption onto the Mg_4Fe and Mg_4Fe-450 materials was an endothermic process, due to the obtained positive value for ΔH^o, and spontaneous because the Gibbs free energy presented negative values, which decreased as the temperature increased. Also, the positive values for ΔH^o and ΔS^o suggest that, during the adsorption process, the solid–liquid interface increases the randomness and the adsorption takes place due to chemical interactions [41].

3.5. Adsorption Performance

The adsorption performances of the synthesized materials developed in the removal process of MoO_4^{2-} adsorption from aqueous solutions were compared with the adsorption capacities developed by similar materials that were reported in the literature. The results are presented in Table 6, and it can be observed that Mg/Fe–LDH obtained from secondary sources can be efficiently used as an adsorbent material for treatment of water with dissolved Mo(VI).

Table 6. The comparison between the adsorption capacities of similar adsorbents developed for the treatment processes of aqueous solutions containing MoO_4^{2-} anions.

Adsorbent	q_m mg/g	References
Zn_3Al–CO_3-LDH	13.7	[2]
Zn_3Al-CLDH	39.8	
$ZnAl_3$–Cl-LDH	114.9	[8]
$ZnAl_3$–CO_3-LDH	<10	
$MgFeSO_4$-type HT-LDH	15.5	[42]
Mg_4Fe	42.1	Present paper
Mg_4Fe-450	55.2	

After adsorption, the solid materials were recovered by filtration and were subjected to XRD analysis. The XRD patterns of the Mg_4Fe and Mg_4Fe-450 are presented in Figure 11.

The as-synthesized material, Mg_4Fe, did not suffer any change in its crystalline structure after adsorption, with the unit cell parameters being a = 3.11 Å and c = 24.0 Å (compared to the unit cell parameters before adsorption: a = 3.11 Å and c = 23.9 Å). The 003 reflection was almost the same for Mg_4Fe before adsorption ($d_{(003)}$ = 7.967 Å) and after adsorption ($d_{(003)}$ = 8.000 Å). This demonstrates that the adsorption of Mo(VI), as molybdate anions, was performed on the LDH surface and not through anion exchange, considering that carbonate is the most difficult to replace among the anions present in the LDH interlayer gallery. On the other hand, as shown in Figure 11, the calcined material, Mg_4Fe-450, regained its layered double hydroxide structure, and all the characteristic peaks of pyroaurite were present in the diffractogram. The unit cell parameters of Mg_4Fe-450 after adsorption (a = 3.12 Å and c = 24.7 Å) suggest that the rehydration process of the calcined material (the memory effect) was developed

through adsorption of Mo(VI) as molybdate anions from the solution and incorporated in the interlayer space of LDH. Furthermore, $d_{(003)}$ for Mg_4Fe-450 after adsorption increased to 8.233 Å. This increase in basal spacing indicates that molybdate anions were intercalated into the interlayer spaces of the reformed LDH. During Mo(VI) adsorption onto the calcined sample, instead of carbonate ions from the atmosphere, Mo(VI) anions were intercalated from the solutions due to the fact that the anion volume of Mo(VI) is higher than that of carbonate (V_{MoO4}^{2-} = 0.088 nm^3; V_{CO3}^{2-} = 0.061 nm^3) [43]. The retention of Mo(VI) through the memory effect between the interlayer gallery and also through adsorption onto the layer of the Mg_4Fe-450 surface explain the higher adsorption capacity developed by this material compared with its precursor. These results agree with other results reported in the literature [34,44].

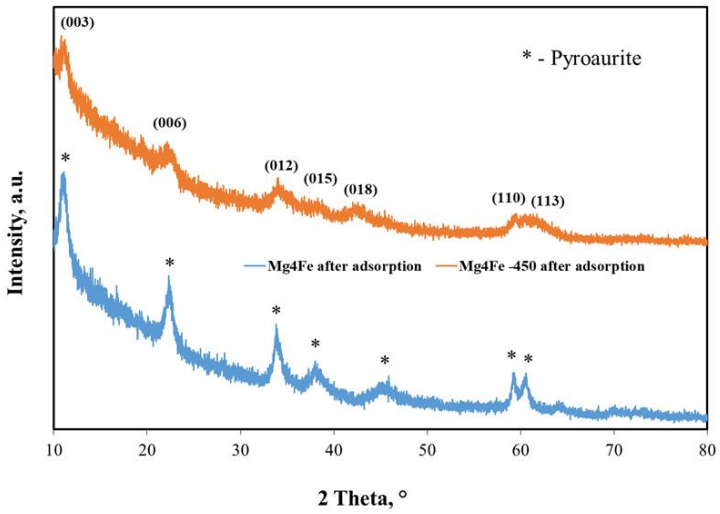

Figure 11. XRD patterns of the materials after Mo(VI) adsorption.

The morphology of the samples after Mo(VI) adsorption can be observed from the TEM images presented in Figure 12. The specific hexagonal morphology with ultrathin layers for the LDH samples can be observed in the presented TEM images. Due to their small crystallite size and the fact that it is difficult to isolate a unique crystal, the formation of some aggregates can be observed. The calcined sample, through the memory effect after Mo(VI) adsorption, returned to the hexagonal shape specific to LDH due to reformation of the layer structures.

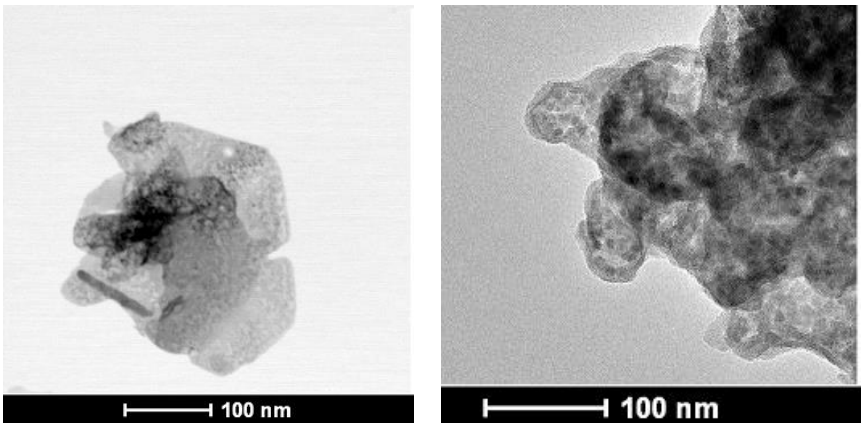

(**a**) (**b**)

Figure 12. TEM images of the materials after Mo(VI) adsorption: (**a**) Mg_4Fe and (**b**) Mg_4Fe-450.

4. Conclusions

This paper reports the successful synthesis of a new Mg_4Fe–LDH using, as iron precursor, a secondary source, namely, the acidic residual solution resulting from the pickling step of the hot-dip galvanizing process. The obtained LDH presented similar properties to those obtained from pure reagents. The impurities present in the residual solutions, besides the iron ions, did not interfere with the structure of the obtained LDH. The obtained Mg_4Fe and the calcined product presented efficient adsorption properties in the removal process of MoO_4^{2-} from aqueous solutions. The proposed method of obtaining LDH presents multiple benefits: (1) it decreases the cost of obtaining LDH; (2) it decreases the cost of acidic residual solution neutralization; (3) it reduces waste discharge into the environment, and (4) it minimizes the use of raw materials.

Author Contributions: Conceptualization, L.L. and R.P.; methodology, L.C.; formal analysis, A.G. and L.L.; investigation, A.G., L.L. and L.C.; writing—original draft preparation, L.L. and R.P.; writing—review and editing, L.L. and L.C.; visualization, L.C.; supervision, R.P.

Funding: This research received no external funding.

Acknowledgments: The studies were done during the PhD program from the Doctoral School of the University Politehnica Timisoara.

Conflicts of Interest: The authors declare no conflict of interest.

References

1. Dore, E.; Frau, F.; Cidu, R. Antimonate Removal from Polluted Mining Water by Calcined Layered Double Hydroxides. *Crystals* **2019**, *9*, 410. [CrossRef]
2. Cocheci, L.; Lupa, L.; Lazau, R.; Voda, R.; Pode, R. Zinc recovery from waste zinc ash—A new "green" route for the preparation of Zn-Al layered double hydroxide used for molybdate retention. *J. Alloys Compd.* **2019**, *787*, 332–343. [CrossRef]
3. Lupa, L.; Cocheci, L.; Pode, R.; Hulka, I. Phenol adsorption using Aliquat 336 functionalized Zn-Al layered double hydroxide. *Sep. Pur. Technol.* **2018**, *196*, 82–95. [CrossRef]
4. Cavani, F.; Trifiro, F.; Vaccari, A. Hydrotalcite-type anionic clays: Preparation, properties and applications. *Catal. Today* **1991**, *11*, 173–301. [CrossRef]
5. Asiabi, H.; Yamini, Y.; Shamsayei, M.; Tahmasebi, E. Highly selective and efficient removal and extraction of heavy metals by layered double hydroxides intercalated with the diphenylamine-4-sulfonate: A comparative study. *Chem. Eng. J.* **2017**, *323*, 212–223. [CrossRef]
6. Carriazo, D.; del Arco, M.; Martin, C.; Rives, V. A comparative study between chloride and calcined carbonate hydrotalcites as adsorbents for Cr (VI). *Appl. Clay Sci.* **2007**, *37*, 231–239. [CrossRef]
7. Ardau, C.; Frau, F.; Dore, E.; Lattanzi, P. Molybdate sorption by Zn-Al sulphate layered double hydroxides. *Appl. Clay Sci.* **2012**, *65–66*, 128–133. [CrossRef]
8. Koilraj, P.; Srinivasan, K. ZnAl layered double hydroxides as potential molybdate sorbents and valorise the exchanged sorbent for catalytic wet peroxide oxidation of phenol. *Ind. Eng. Chem. Res.* **2013**, *52*, 7373–7381. [CrossRef]
9. Ashekuzzaman, S.M.; Jiang, J.Q. Strategic phosphate removal/recovery by a re-usable Mg-Fe-Cl layered double hydroxide. *Process. Saf. Environ. Prot.* **2017**, *107*, 454–462. [CrossRef]
10. Wan, S.; Wang, S.; Li, Y.; Gao, B. Functionalizing biochar with Mg-Al and Mg-Fe layered double hydroxides for removal of phosphate from aqueous solutions. *J. Ind. Eng. Chem.* **2017**, *47*, 246–253. [CrossRef]
11. Ogata, F.; Nagai, N.; Kishida, M.; Nakamura, T.; Kawasaki, N. Interaction between phosphate ions and Fe-Mg type hydrotalcite for purification of wastewater. *J. Environ. Chem. Eng.* **2019**, *7*, 102897. [CrossRef]
12. Matsuik, J.; Rybka, K. Removal of chromates and sulphates by Mg/Fe LDH and heterostructured LDH/Halloysite materials: Efficiency, selectivity, and stability of adsorbents in single and multi-element systems. *Materials* **2019**, *12*, 1373. [CrossRef] [PubMed]
13. Caporale, A.G.; Pigna, M.; Azam, S.M.G.G.; Sommella, A.; Rao, M.A.; Violante, A. Effect of competing ligands on the sorption/desorption of arsenite on/from Mg-Fe layered double hydroxides (Mg-Fe-LDH). *Chem. Eng. J.* **2013**, *225*, 704–709. [CrossRef]

14. Xie, Y.; Yuan, X.; Wu, Z.; Zeng, G.; Jiang, L.; Peng, X.; Li, H. Adsorption behaviour and mechanism of Mg/Fe layered double hydroxide with Fe_3O_4-carbon sphere on the removal of Pb(II) and Cu(II). *J. Coll. Interf. Sci.* **2019**, *536*, 440–455. [CrossRef]
15. Das, J.; Sairam Patra, B.; Baliarsingh, N.; Parida, K.M. Calcined Mg-Fe-CO_3 LDH as and adsorbent for the removal of selenite. *J. Coll. Interf. Sci.* **2007**, *316*, 216–223. [CrossRef]
16. Hudcova, B.; Erben, M.; Vitkova, M.; Komarek, M. Antimonate adsorption onto Mg-Fe layered double hydroxides in aqueous solutions at different pH values: Coupling surface complexation modelling with solid-state analyses. *Chemosphere* **2019**, *229*, 236–246. [CrossRef]
17. Ahmed, I.M.; Gasser, M.S. Adsorption study of anionic reactive dye from aqueous solution to Mg-Fe-CO_3 layered double hydroxides (LDH). *Appl. Surf. Sci.* **2012**, *259*, 650–656. [CrossRef]
18. Ayawei, N.; Angaye, S.S.; Wankasi, D. Mg/Fe layered double hydroxide as a novel adsorbent for the removal of Congo red. *Int. J. Appl. Sci. Technol.* **2017**, *7*, 83–92.
19. Abdelkader, N.B.-H.; Bentouami, A.; Derriche, Z.; Bettahar, N.; de Ménorval, L.-C. Synthesis and characterization of Mg–Fe layer double hydroxides and its application on adsorption of Orange G from aqueous solution. *Chem. Eng. J.* **2011**, *169*, 231–238. [CrossRef]
20. Zhang, S.; Jiao, Q.; Wang, C.; Yu, H.; Zhao, Y.; Li, H.; Wu, Q. In situ synthesis of Mg/Fe LDO/carbon nanohelix composites as adsorbing materials. *J. All. Comp.* **2016**, *658*, 505–512. [CrossRef]
21. Tahir, N.; Abdelssadek, Z.; Halliche, D.; Saadi, A.; Chebout, R.; Cherifi, O.; Bachari, K. Mg-Fe-hydrotalcite as catalyst for the benzylation of benzene and other aromatics by benzyl chloride reactions. *Surf. Inter. Anal.* **2008**, *40*, 254–258. [CrossRef]
22. Chang, P.S.; Li, S.Y.; Juang, T.Y.; Liu, Y.C. Mg-Fe layered double hydroxides enhance surfactin production in bacterial cells. *Crystals* **2019**, *9*, 355. [CrossRef]
23. Muriithi, G.N.; Petrik, L.F.; Gitari, W.M.; Doucet, F.J. Synthesis and characterization of hydrotalcite from South Africa Coal fly ash. *Powder Technol.* **2017**, *312*, 299–309. [CrossRef]
24. Cocheci, L.; Lupa, L.; Gheju, M.; Golban, A.; Lazau, R.; Pode, R. Zn–Al–CO_3 layered double hydroxides prepared from a waste of hot-dip galvanizing process. *Clean Technol. Environ. Policy* **2018**, *20*, 1105–1112. [CrossRef]
25. Kuwahara, Y.; Yamashita, H. Synthesis of Ca-based layered double hydroxide from blast furnace slag and its catalytic applications. *ISIJ Intern.* **2015**, *7*, 1531–1537. [CrossRef]
26. Galindo, R.; Lopez-Delgato, A.; Padilla, I.; Yates, M. Hydrotalcite-like compounds: A way to recover a hazardous waste in the aluminium tertiary industry. *Appl. Clay Sci.* **2014**, *95*, 41–49. [CrossRef]
27. Murayama, N.; Maekawa, I.; Ushiro, H.; Miyoshi, T.; Shibata, J.; Valix, M. Synthesis of various layered double hydroxides using aluminium dross generated in aluminium recycling process. *Int. J. Miner. Process.* **2012**, *110–111*, 46–52. [CrossRef]
28. Golban, A.; Cocheci, L.; Lazau, R.; Lupa, L.; Pode, R. Iron ions reclaiming from sludge resulted from hot-dip galvanizing process, as Mg_3Fe-layered double hydroxide used in the degradation process of organic dyes. *Des. Water Treat.* **2018**, *131*, 317–327. [CrossRef]
29. Panayotova, M.; Panayotov, V. An Electrochemical Method for Decreasing the Concentration of Sulfate and Molybdenum Ions in Industrial Wastewater. *J. Environ. Sci. Health Part A-Toxic/Hazard. Subst. Environ. Eng.* **2004**, *39*, 173–183. [CrossRef]
30. Lievens, P.; Block, C.; Cornelis, G.; Vandecasteele, C.; De Voogd, J.C.; Van Brecht, A. Mo, Sb and Se Removal from Scrubber Effluent of a Waste Incinerator. In *Water Treatment Technologies for the Removal of High-Toxicity Pollutants*; Vaclavikova, M., Vitale, K., Gallios, G.P., Ivanicova, L., Eds.; Springer: Dordrecht, The Netherlands, 2010.
31. Verbinnen, B.; Block, C.; Hannes, D.; Lievens, P.; Vaclavikova, M.; Stefusova, K.; Gallios, G.; Vandecasteele, C. Removal of molybdate anions from water by adsorption on zeolite-supported magnetite. *Water Environ. Res.* **2012**, *84*, 753–760. [CrossRef]
32. World Health Organization (WHO). Guidelines for Drinking-Water Quality, Fourth Edition. 2011. Available online: http://whqlibdoc.who.int/publications/2011/9789241548151_eng.pdf (accessed on 2 September 2019).
33. Underwood, E.J. *Trace Elements in Human and Animal Nutrition*, 3rd ed.; Academic Press: London, UK, 1971.
34. Palmer, S.J.; Soisonard, A.; Frost, R.I. Determination of the mechanism(s) for the inclusion of arsenate, vanadate or molybdate anions into hydrotalcites with variable cationic ratio. *J. Colloid Interface Sci.* **2009**, *329*, 404–409. [CrossRef] [PubMed]

35. Tkac, P.; Paulenova, A. Speciation of molybdenum (VI) in aqueous and organic phases of selected extraction systems. *Sep. Sci. Technol.* **2008**, *43*, 2641–2657. [CrossRef]
36. Pietrelli, L.; Ferro, S.; Vocciante, M. Raw materials recovery from spent hydrochloric acid-based galvanizing wastewater. *Chem. Eng. J.* **2018**, *341*, 539–546. [CrossRef]
37. Ferreira, O.P.; Alves, O.L.; Gouveia, D.X.; Souza Filho, A.G.; de Paiva, J.A.C.; Mendes Filho, J. Thermal decomposition and structural Reconstruction effect on Mg–Fe based hydrotalcite compounds. *J. Solid State Chem.* **2004**, *177*, 3058–3069. [CrossRef]
38. Elmoubarki, R.; Mahjoubi, F.Z.; Elhalil, A.; Tounsadi, H.; Abdennouri, M.; Sadiq, M.; Qourzal, S.; Zouhri, A.; Barka, N. Ni/Fe and Mg/Fe layered double hydroxides and their calcined derivatives: Preparation, characterization and application on textile dyes removal. *J. Mat. Res. Technol.* **2017**, *6*, 271–283. [CrossRef]
39. Dada, A.O.; Olalekan, A.P.; Olatunya, A.M.; Dada, O. Langmuir, Freundlich, Temkin and Dubinin–Radushkevich isotherms studies of equilibrium sorption of Zn^{2+} unto phosphoric acid modified rice husk. *IOSR-JAC* **2012**, *3*, 38–45.
40. Ertugay, N.; Malkoc, E. Adsorption isotherm, kinetic, and thermodynamic studies for methylene blue from aqueous solution by needles of Pinus sylvestris L. *Pol. J. Environ. Stud.* **2014**, *23*, 1995–2006.
41. Zhang, L.; Huang, T.; Zhang, M.; Guo, X.; Yuan, Z. Studies on the capability and behavior of adsorption of thallium on nano-Al_2O_3. *J. Hazard. Mater.* **2008**, *157*, 352–357. [CrossRef]
42. Paikaray, S.; Hendry, M.J.; Essilfie-Dughan, J. Controls on arsenate, molybdate, and selenate uptake by hydrotalcite-like layered double hydroxides. *Chem. Geol.* **2013**, *345*, 130–138. [CrossRef]
43. Jenkins, H.D.B.; Roobottom, H.K.; Passmore, J.; Glasser, L. Relationships among ionic lattice energies, molecular (formula unit) volumes, and thermochemical radii. *Inorg. Chem.* **1999**, *38*, 3609–3620. [CrossRef]
44. Smith, H.D.; Parkinson, G.M.; Hart, R.D. In situ absorption of molybdate and vanadate during precipitation of hydrotalcite from sodium aluminate solutions. *J. Cryst. Grow.* **2005**, *275*, e1665–e1671. [CrossRef]